"International Multidimensional Engine Modeling User's Group Meeting at the SAE Congress"
The Detroit Downtown Courtyard by Marriott Hotel, Detroit, MI (USA), April 11^{th}, 2016

Hybrid RANS/LES of Moving Boundary Problems: Application to Cavitating Sprays and In-Cylinder Flows

F. Piscaglia, A. Montorfano, Y. Wu, J. Martínez, F. Giussani, A. Onorati
Politecnico di Milano, Italy

J. Hélie
Continental Automotive SAS, Tolouse, France

S. M. Aithal
Argonne National Laboratory, Lemont, IL 60439, United States

High-fidelity simulations of turbulent flows require highly resolved grids, leading to unacceptably large computational wall-time even on large supercomputers. In an attempt to address these conflicting constraints, we propose the use of a hybrid LES/RANS scale-adaptive turbulence model, where a novel formulation of a dynamic filter allows to define what can be resolved by the computational grid and time step on the basis of the modeled length and time scales. The approach greatly reduces the overall grid-points in the simulation while also fully resolving regions of high-turbulence. A previously developed algorithm for dynamic mesh generation with topological changes was enhanced and coupled with fast, robust compressible segregated flow solvers. These algorithmic developments were made keeping in mind important considerations of load-balancing in order to achieve good strong scaling on modern supercomputers. Massively parallel simulations, which ran on up to 1024 cores on the supercomputers at Argonne National Lab, were conducted on several different test-cases: the dynamic VOF simulation of multi-hole high-pressure injector, a square piston engine with a guillotine moving valve and test cases from the ERCOFTAC database.

INTRODUCTION

This paper discusses extensions and enhancements to a C++ dynamic library for the parallel simulation of time-resolved turbulence modeling of unsteady flows over dynamic grids in general CFD problems [**?**, **?**, **?**, **?**, **?**, **?**, **?**, **?**, **?**]. Code development is done in the OpenFOAM® technology and it is compatible with the most updated release of the code, namely, the "dev" version by H. Weller [**?**]. The paper discusses the most recent code development by the authors in the period June 2015-March 2016, that have been mainly focused on:

- methods to improve temporal accuracy when second order temporal schemes are combined with dynamic addition and removal of cell layers;
- enhanced formulation of the momentum interpolation method (MIM) in the pressure-velocity coupling algorithm, to reduce solution-dependence on under-relaxation factors and time-step advancement in segretated solvers;
- algorithms to perform balanced constraint domain decomposition with mesh motion, to enhance code performance in massively parallel simulations;
- enhancements to the mesh motion handling to achieve faster operation in dynamic simulations based on non-conformal grids; the simulation of in-cylinder flows in 2-stroke engines is used as example of such application;
- turbulence modeling: implementation of the adaptive filtering of the turbulence scales in space and time [**?**] has been extended to be applied to any combination of RANS and LES models;
- multiphase dynamic VOF (Volume Of Fluid) solvers for the simulation of internal nozzle cavitating flows in high-pressure GDI gasoline injectors, during the valve opening and closure events.

The developed code has been validated on two different cases:

- a square piston executing a sinusoidal motion in a square compression chamber with large optical accesses [**?**, **?**], where gases flow in and out of the chamber through a plane channel that can be closed in phase with piston motion cycles. This device mimics a four-stroke-like cycle with intake, compression, expansion and exhaust; also, such a geometrical configuration creates a large-scale vortex tumble during the inlet stroke. This experiment is representative of flows in automotive engines in term of tumble behaviour, volumetric ratio and tumbling number and hence a reliable test case for the validation of turbulence models.
- the Continental XL3.0 6-hole injector, a real multi-hole injector prototype especially developed for investigations in the framework of the collaborative project FUI MAGIE. The test case is used for validation and testing of the dynamic VOF solver, used for the study of flow cavitation in internal nozzle flows and primary jet atomization. For this case, highly-resolved meshes are

required to accurately capture the physics of phase-change in cavitating flows in internal injector nozzles which greatly limits the size of time-steps. Given these considerations, the use of large-scale computing is imperative to reduce the overall wall-time. In order to achieve high-scalabililty on large computing clusters, special attention has to be paid to the decomposition strategy and to the code development, to ensure good load balancing minimizing communication among processors. The strategy followed to achieve good scalability on large scale problems and performance analyses for various grid-sizes (ranging from 1M to 64M) from 16 to 1024 cores on an Intel Sandy bridge processors is discussed.

COMPRESSIBLE DYNAMIC SOLVER

A newly developed unsteady transient solver family named `TopoDyM`, supporting dynamic grids with topological changes has been employed. In particular, common features to all the solvers include:

- enhanced method for face-flux correction with topological changes and strict coupling between pressure and energy [**?**, **?**];
- implementation of a corrected Momentum Interpolation Method (MIM) [**?**] in the pressure-velocity coupling algorithm, to ensure solution independence on the under-relaxation factor in the inner iteration of the transient SIMPLE algorithm, that is discussed here.

In the original versions of the solvers implemented in OpenFOAM®, the Rhie and Chow technique for momentum-based interpolation of mass fluxes on cell faces (OMIM) is used for staggered-grid discretization:

$$u_e = \overline{h_e} - \alpha_u \overline{\left(\frac{1}{A_e}\right)} \Delta y (p_E - p_P) \qquad (1)$$

where α_u is the velocity under-relaxation factor, Δy is the vertical spacing of cell P and the over-bar denotes linear interpolation of cell values (E and P) in the shared face e. The term $\overline{h_e}$ is the face interpolation of h_P, a matrix which includes all off-diagonal ($\sum_{nb} A_{nb} u_{nb}$) and source terms (b_P) of the under-relaxed velocity equations and reads: $h_P = \left(\alpha_u \left(\sum_{nb} A_{nb} u_{nb} + b_P\right)_P\right) / \left((A_P)_P\right) + (1-\alpha_u) u_P^0$, being A_P the diagonal coefficient and u_P^0 the cell velocity in the previous iteration. The OMIM resolves one of the main problems with colocated grids, namely, the checker-board pressure field, that would appear when the pressure gradient term is discretized in the momentum equations. While the OMIM resolves the checker-board problem, it presents additional numerical issues; in particular, Majumdar [**?**] and Miller et al. [**?**] independently reported that solutions obtained with the OMIM are under-relaxation factor-dependent. The proposed correction, referred to as the Majumdar Momentum Interpolation Method (MMIM), consists of a reformulation of the face velocities used in the pressure equation as follows:

$$u_e = \overline{h_e} + \alpha_u \overline{\left(\frac{1}{A_e}\right)} \Delta y (p_E - p_P) + (1-\alpha_u) \left[u_e^0 - \overline{u_e^0}\right] \qquad (2)$$

The implementation of the MMIM has been validated on steady RANS simulation of a turbulent ($Re \approx 6 \cdot 10^6$, based on the chord length) incompressible flow ($M = 0.15$) around a NACA0012 profile. The choice to perform the validation of the implementation on a steady case is due to the consideration that the inner iteration of transient-SIMPLE based solvers (`PIMPLE`) is a pure SIMPLE iteration; also, in a steady case the influence of the time-step marching is not included in the solution [**?**]. Experimental measurements for pressure distribution C_p, lift coefficient C_L and drag coefficient C_D in upper wall for different angles of attack β were considered for comparison with numerical solutions. A structured C-grid has been used for the simulations. Freestream turbulence intensity of 0.052% and turbulence viscosity ratio $\nu_t/\nu = 0.009$ have been used to set the appropriate boundary conditions.

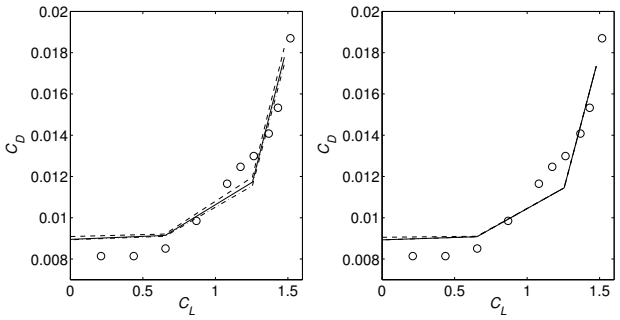

Figure 1: C_D coefficient determined for OMIM (left) and MMIM (right) for several angles of attack β: 0, 6, 12 and 15 degrees. Results are shown for $\alpha_u = 0.2$ ($---$); $\alpha_u = 0.5$ (—); $\alpha_u = 0.8$ ($- \cdot -$) in comparison with epxerimental data ($\circ$).

The effect of changing the under-relaxation factor α_u on velocity was studied, while maintaining the pressure under-relaxation $\alpha_p = 1 - \alpha_u$ and the under-relaxation on turbulence quantities fixed. While C_L and C_p were not sensitive to variations of α_u with any momentum interpolation method, Fig. 1 shows how results for C_D change significantly with α_u, when the OMIM is used. Small variations in velocity fields produce larger variations in velocity gradients (and therefore in the drag forces), while C_L, mainly influenced by pressure force is not notably affected. A detailed comparison between the performance of the different interpolation methods in the solver is reported in Tab. 1: the correction to Eq. (1) introduced in (2) allows to reduce the relative change of the predicted values with α_u up to two orders of magnitude.

Table 1: Dependency of C_D, C_L on α_u

Coefficient		OMIM	MMIM
C_L	$\alpha_u = 0.2$	1.2543421	1.2554539
	$\alpha_u = 0.8$	1.2552675	1.2554399
	Rel. Change	0.133 %	0.001%
C_D	$\alpha_u = 0.2$	0.011948155	0.011446795
	$\alpha_u = 0.8$	0.011549183	0.011451306
	Rel. Change	3.339 %	0.039%

With MMIM, the reduction of the dependency is related to the level of convergence acquired in the simulations and therefore the effect is particularly apparent as coarse grids are used. For more detailed discussion on this part of the work, please refer to [**?**].

TURBULENCE MODELING

A detailed explanation of the theory of the scale adaptive filtering technique applied for turbulence and its validation can be found in [?].

THE COMPRESSED VORTEX CASE

The compressible single phase solver `topoEngineFoam` was used to simulate the configuration described in Fig. 2; measurements for validation were made available by Prof. Borée, by ISAE-ENSMA [?]. As described earlier, this case consists of a square piston executing a sinusoidal motion in a square compression chamber. A large plenum (not shown in the picture) is connected to the intake channel to absorb pressure oscillations.

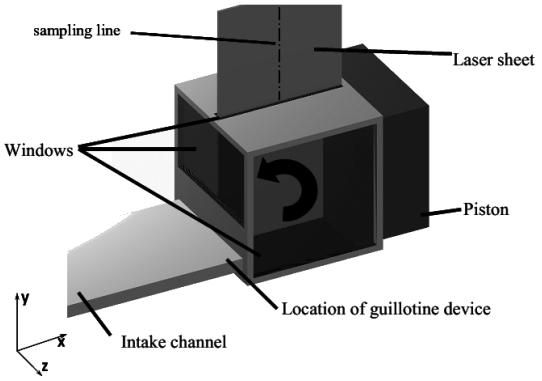

Figure 2: Sketch of experimental set up. 2D-PIV is done on the laser sheet passing through the cylinder axis; data for graph are sampled along the y-axis in the middle of the plane.

The piston has square shape with $l = 100$ mm moving with a sinusoidal frequency of 3.43 Hz; stroke is 75 mm and head clearance at Top Dead Center is 25 mm, leading to a volumetric compression ratio $r = 4$. Two-dimensional PIV measurements are available on a plane passing through the piston axis, as shown in Fig. 2; for each engine phase 120 samples were imaged. The engine operates under two different modes, showed in Fig. 3:

- a "compressed" or "moving valve" mode, where the guillotine moves up and down to mimic the stages of a four-stroke engine (Fig. 3, left);
- an "uncompressed" or "open valve" mode, in which the guillotine is constantly open (Fig. 3, right).

Hybrid RANS/LES simulations was carried out and internal flow fields in the engine working under both "moving valve" and "open valve" modes were monitored and compared with the experiments. The grids used for the simulations are shown in Fig. 3. For the open-valve mode, the mesh has a cell number ranging from 1.1 M at the piston TDC to 2.4M when the piston is at BDC; a coarser mesh, with a cell number varying from 0.23 million (TDC) to 0.4 million (BDC) was used for the simulation of the engine with moving valve. The choice of using a coarser mesh in the dynamic simulation was to reduce the overall computational time for a time resolved simulation and to test the performance of the hybrid DLRM model [?] on grids suitable for RANS simulation.

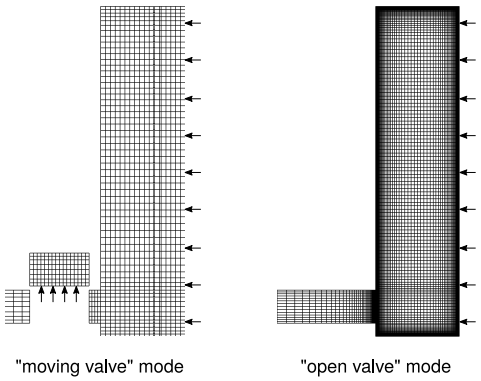

Figure 3: Different working modes of the square-piston engine: "compressed" or "moving valve" mode (left); "uncompressed" or "open valve" mode (right). The mesh shown are those used in the simulations.

Automatic mesh motion handling based on topological changes was accomplished by the C++ class `engineTopoMesh` [?, ?] which extends the capability of OpenFOAM®, in the version released by the OpenFOAM® Foundation. Cell layers are dynamically and automatically added or removed over the piston during its motion, while the guillotine is a volume chamber that is connecting (or disconnecting) the cylinder volume with the intake duct. In the code, the moving guillotine is modelled as a fluid-dynamic region having a prescribed motion, that is dynamically connected/disconnected to the remaining fluid-dynamic domain by non-conformal sliding interfaces. Further details about the code implementation of the `slidingInterface` mesh modifier used are included in [?, ?].

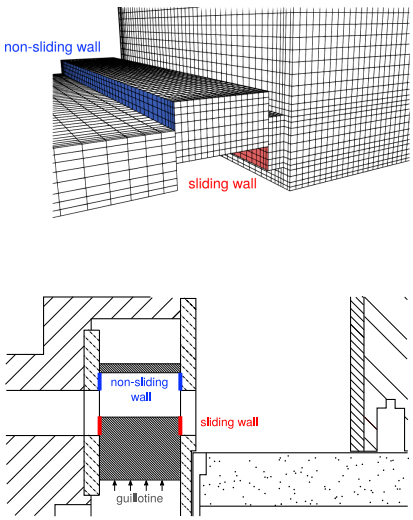

Figure 4: Detail of the guillotine mesh: Finite Volume mesh (top); experimental setup (bottom).

In the simulations with the moving guillotine ("moving valve" mode), particular care was taken to model the guillotine and its boundaries, as shown in Fig. 3 (left) and Fig. 4. Wall boundaries marked in red in Fig. 4 have a non-zero tangential velocity; conversely, the upper walls of the guillotine "chamber" (in blue in Fig. 4) are fixed in the real configuration, so their velocity would be zero at the walls. In order to enforce a realistic boundary condition on these surfaces, the guillotine velocity was set at run-time on the

sliding faces of the moving grid (Fig. 4, top): in the code, the list of faces belonging to the red and blue area of Fig. 4 is dynamically updated at each crank time angle and:

- a Dirichlet boundary condition $\vec{u} = 0$ is set on the fluid velocity in the area that would be fixed in the real configuration (blue area in Fig. 4);
- a Neumann boundary conditions $\frac{d\vec{u}}{d\vec{n}} = 0$ is set on fluid velocity for the side faces that would correspond to the moving region in the real configuration (red area in Fig. 4).

Moreover, the attach/detach procedure of the `slidingInterface` [**?**] has been slightly improved with respect to the first version. When the valve is either in "fully open" or "fully closed" position, operation of the sliding interface is deactivated and the interface becomes static. This allows for a noticeable reduction of the computational cost, for the attach/detach of a sliding interface is indeed computationally expensive, even when it involves no actual topology change.

Eleven "open valve" mode cycles and nine "moving valve" mode cycles were simulated; for each of these cases, the first two cycles were discarded as they served as initialization of the overall flow fields. Validation was carried out by comparing phase-averaged velocities and RMS of turbulent fluctuations on the PIV plane previously described. A further investigation of coherent structures of the in-cylinder flow by means Proper Orthogonal Decomposition (POD) is presented.

Square piston engine: simulation results

Experimental data from PIV measurements were available on a two-dimensional plane [**?**] passing through the cylinder axis, as shown in Fig. 2. Data were also sampled over a line crossing the plane. 2D phase-averaged velocity and the corresponding turbulence kinetic energy TKE (RMS of the 2-D fluctuating velocity) were then calculated; in the following, they will be referred to as $\overline{\mathbf{U}}$ and k. For each configuration ("open valve" modeand "moving valve" mode), in Fig. 5 and 6 validation of the predicted results is performed for different crank angles on:

- the streamlines of the velocity field, to compare the generic flow structure on the 2d plane;
- the mean velocity, the turbulent intensity and the turbulent kinetic energy calculated over a sample line (see Fig. 2) on the 2d plane.

When the engine works under "open valve" mode, the flow field is dominated by three characteristic structures (Fig. 5: CA=34°, CA=89° and CA=121° deg): the jet formed during the intake stroke, the large scale tumble vortex generated by the redirection of the jet and the small scale vortex in the recirculation area at the lower right corner of the 2D plane. The hybrid turbulence model DLRM is able to capture all these major flow structures with good accuracy. Comparison on a sample line, located at mid distance between the piston and the cylinder head on the 2D plane, also validates the better performance of DLRM against the standard $k-\omega$ SST RAS model (that included the correction for swirling flows). Good agreements were achieved also for the "moving valve" mode, despite the coarse grid for all the crank angles where the measurements were available. Comparison on other crank angles are not shown here for brevity. Proper Orthogonal Decomposition (POD) was performed on both experimental data and simulation results of "open valve" mode. POD decomposes the unsteady flow field into a series of energy containing "modes", each defined by a eigenvalue-eigenvector pair, the former ($\lambda(t)$) related to the energy content of the mode, the latter ($\phi(x)$) defining the "shape" of the same, as shown in Eq. (3):

$$\mathbf{U}(x,t) = \sum_{i=0}^{N} \lambda(t)^{(i)} \cdot \phi(x)^{(i)} + \mathbf{r} \tag{3}$$

where N is the number of POD modes extracted from the results: the higher N, the more complete is the flow description by POD. The "snapshots" method [**?**] has been used because of its lower computational cost when compared with the formal method. Since in-cylinder flow field is driven by a periodically moving boundary, snapshots are collected with a phase-dependent strategy: the number of snapshots, or POD modes, equals the number of engine cycles[**?**]. To keep the consistency of the analysis between simulation and experiment data, 3-D simulation results were mapped onto the 2-D PIV grids on which velocity fields were measured. Eigenvalues of the first 8 modes for all crank-angles are represented in Fig. 8. The energy content of first mode is prevalent over subsequent (higher-order) modes: this is often observed in highly-characterized flows where clear turbulent structures are recognizable. The curve has a maximum at about CA = 90° and minima around Top Dead Centers. This can easily be related to the piston velocity, which is the driving force of the flow. With respect to similar cases (e.g. [**?**]), the energy appears more distributed among modes from 1 to 8; this can be due to a more pronounced turbulent character of the flow. Finally, it should be noted that there is little or no difference between values extracted from simulations and experiments: this confirms the capability of DLRM to predict not only the mean flow statistics, but also its energy content. POD eigenvectors at CA = 121° (intake stroke) are shown in Fig. 7. Good agreement is achieved on "mode 0", which has a strong correlation with the average field as evidenced, for instance, by comparing Fig. 7(a-b) with Fig. 5 (CA=121 ° deg).

Multiphase simulation of internal nozzle flows

In this section, a multi-phase method based on a Volume-of-Fluid (VOF) solver supporting mesh motion based on topological changes and scale-adaptive turbulence modeling is described. This method is applied to simulate atomizing jets under conditions which approximate those found in high-pressure GDI engines. The objectives are to study the physics of jet atomization with cavitation and upstream nozzle geometry induced disturbances, during the injector opening and closing events. The fuel injector geometry modelled has been provided by Continental Automotive SAS and is shown in Fig. 9. Fuel is simulated using n-heptane at $p = 30$ bar and $T = 20$°C; the chamber is filled with fuel vapor (the same that is generated in the nozzle because of cavitation) at an ambient pressure of 1 bar. Simulations of the injector opening event

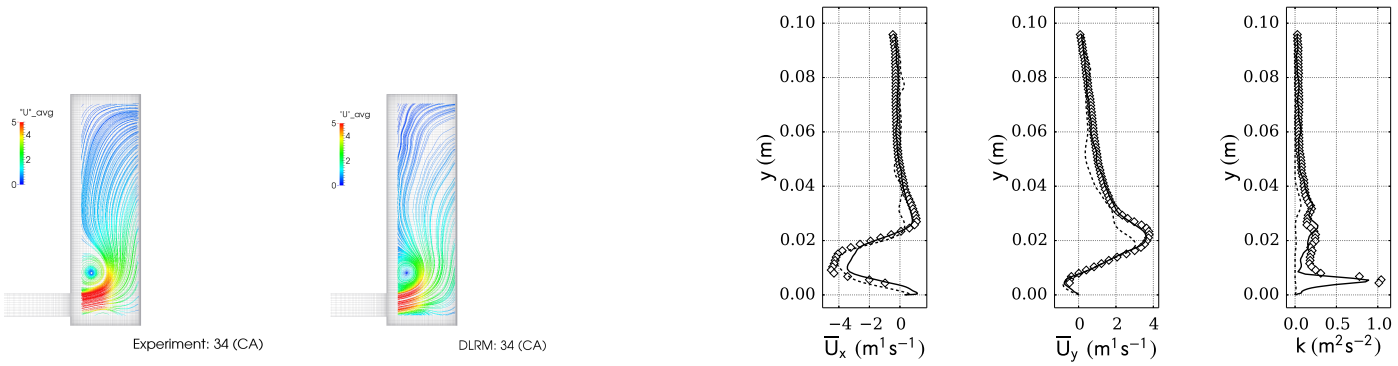

CA = 34° deg

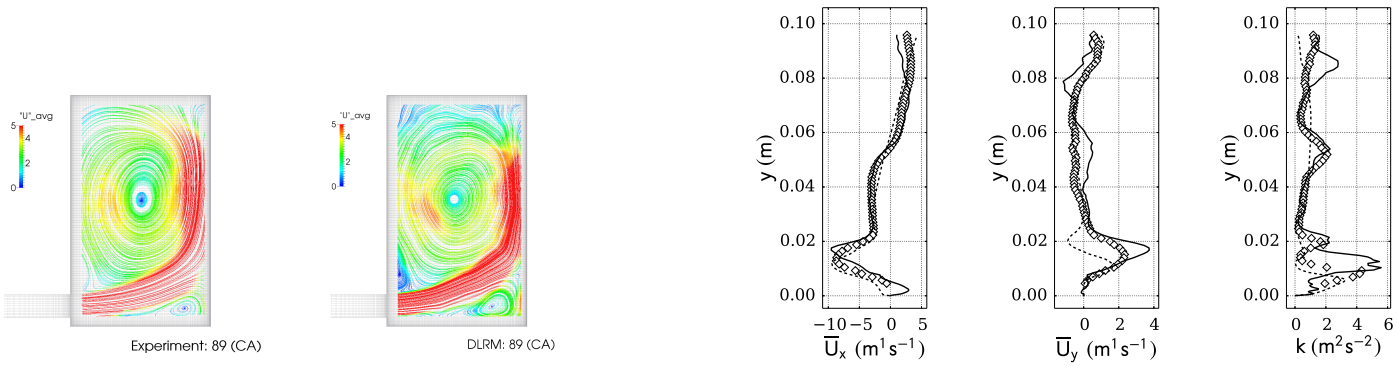

CA = 89° deg

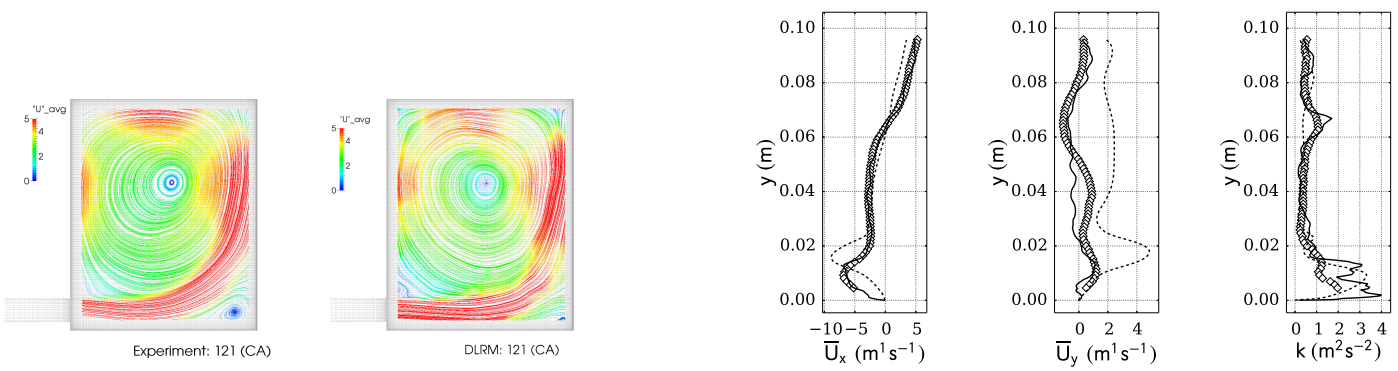

CA = 121° deg

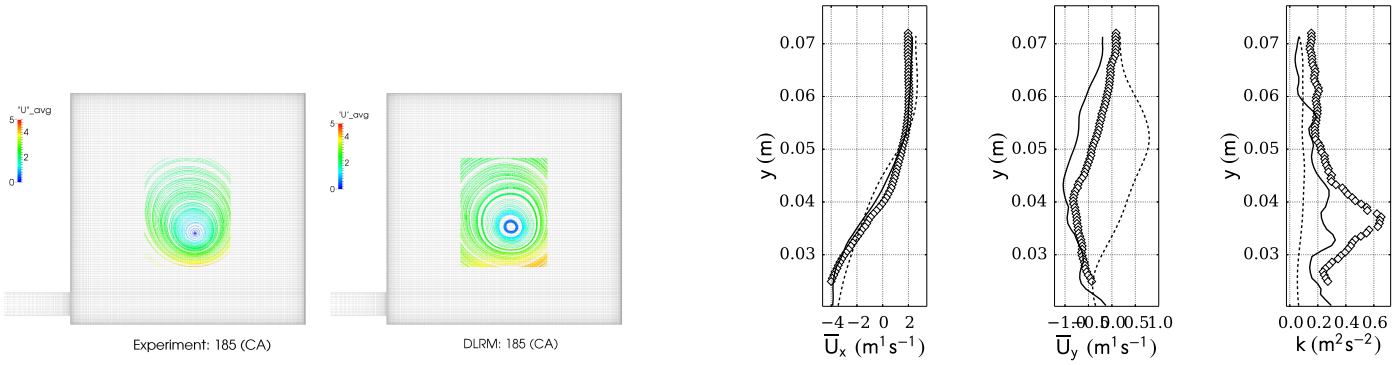

CA = 185° deg

Figure 5: Validation of the DLRM hybrid scale-adaptive model on the square piston geometry at different crank angles ("open valve" mode): streamlines of the velocity flow field (left); Averaged velocity, turbulence intensity and TKE over the sampling line of Fig. 2. Experiments ($\diamond$); $k-\omega$ *SST* RANS (- - -); DLRM (—).

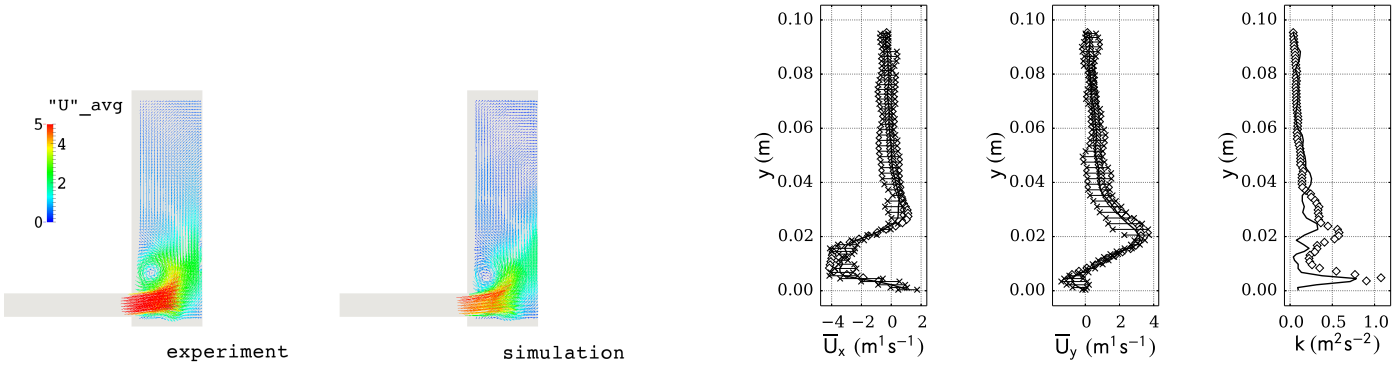

CA = 35° deg

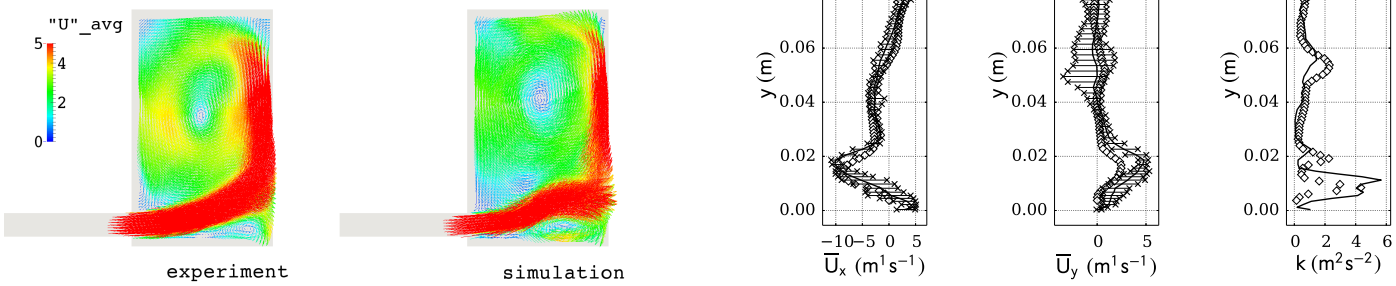

CA = 90° deg

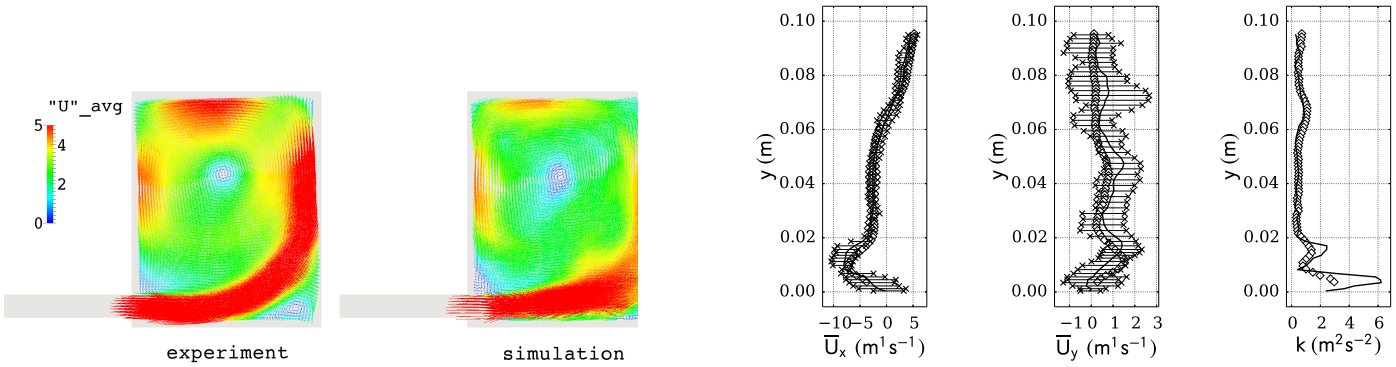

CA = 123° deg

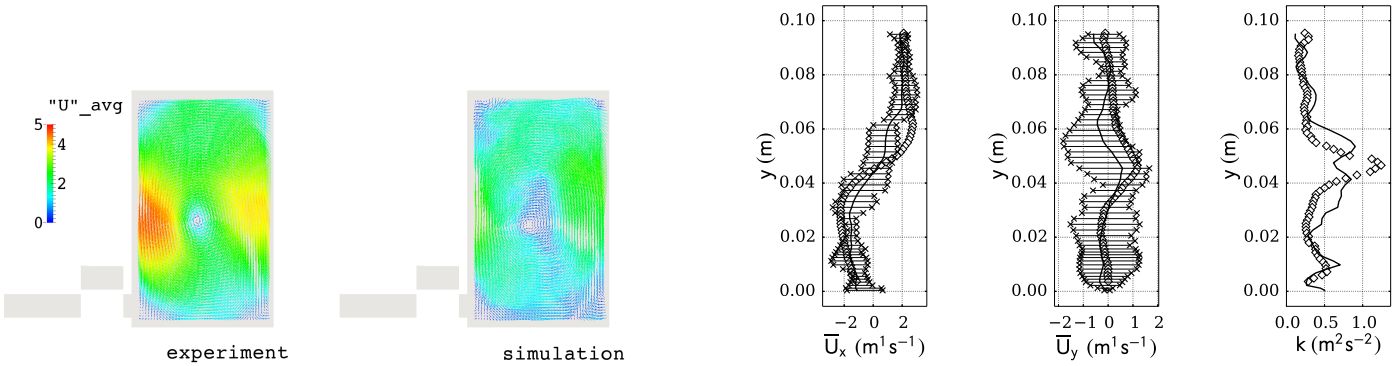

CA = 278° deg

Figure 6: Validation of the DLRM hybrid scale-adaptive model on the square piston geometry at different crank angles ("moving valve" mode): streamlines of the velocity flow field (left); Averaged velocity, turbulence intensity and TKE over the sampling line of Fig. 2. Experiments (⋄); DLRM (—); fluctuation range of DLRM (×).

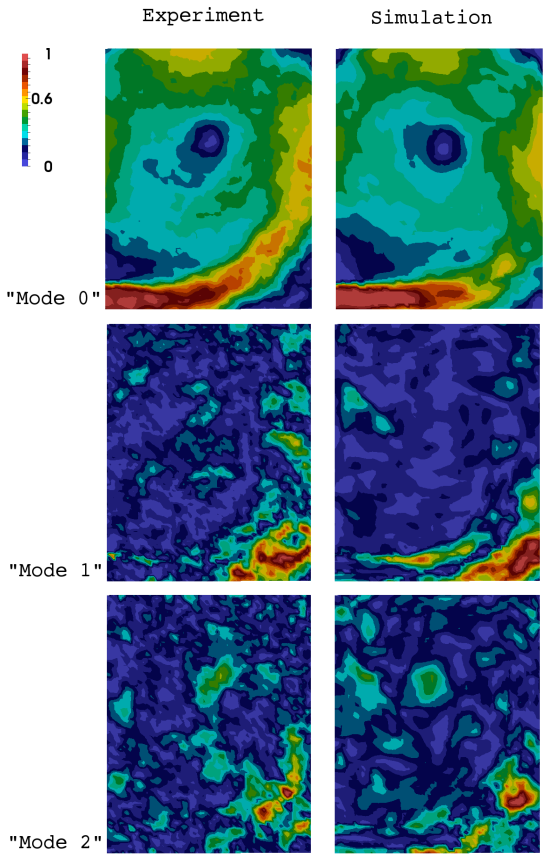

Figure 7: Eigenvectors of first three POD modes; CA = 121°, "Open-valve" operating mode.

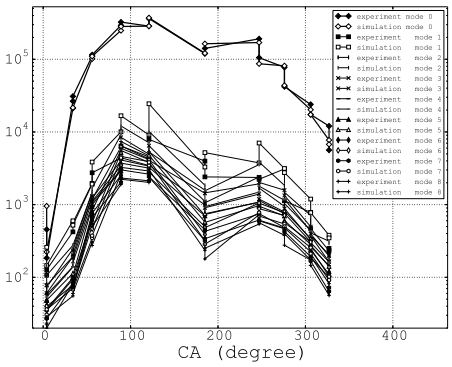

Figure 8: Eigenvalues of first 8 POD modes for different crank-angles. "Open-valve" mode.

have been performed on a computational grid with 12 M cells at the injector closure. The use of a scale-adaptive (hybrid RANS/LES) turbulence model allows for increasing the cell size in the external domain, where velocities are lower and turbulence dynamics is less critical for the global solution; thus the overall number of resulting cells is limited. A multiphase VOF solver has been extended with the moving mesh functionality, to simulate the needle opening and closure events (Fig. 9); a prescribed vertical motion is set for the boundary `needleHead`, while the injector opening/closure event is simulated by dynamically attaching and detaching the conformal interface represented by the set of faces `detachFaces` in Fig. 9. Because of the very small gap between the injector needle and the injector body at closure ($\mathcal{O}(\delta) = 10$ μm), the mesh handling looks particularly difficult: cell sizes change by orders of magnitude during needle movement and a dynamic cell is required to maintain the cell quality. For this reason, dynamic cell layering is applied in two regions of the injector volume over the face sets named as `topFaces` and `bottomFaces`.

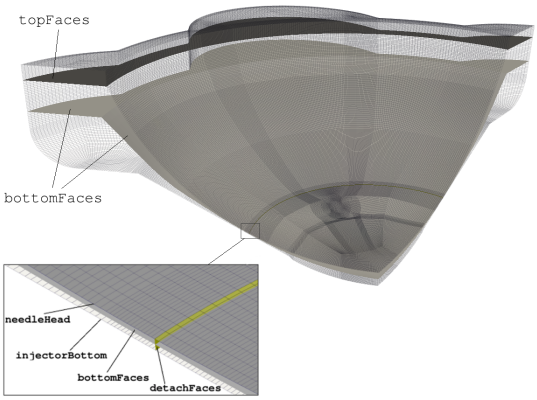

Figure 9: Detail of the Continental XL3.0 6-hole injector, a prototype especially developed for dynamic multiphase-VOF simulations. Dynamic layering is performed by face sets `topFaces` and `bottomFace`; dynamic attach/detach is done on `detachFaces` set; `needleHead` is the moving patch.

To run parallel simulations, the FV mesh has to be decomposed into a set of subdomains, each to be assigned to a single core for processing. In simulations involving mesh motion with topological changes, new constraints in domain decomposition arise: in OpenFOAM®, as well as in most of the CFD codes, topological changes cannot occur across inter-processor patches between neighboring subdomains, so some constraints have to be set on the decomposition algorithm:

- in regions where layer A/R occurs, inter-processor faces cannot be parallel to layer A/R surface;
- both sides of an attach/detach (or sliding interface) modifier must be included in the same subdomain.

Nevertheless, it is important for the decomposition to remain balanced despite the aforementioned restrictions; in addition, the algorithm should require minimal user intervention, allowing the automation of case setup for large simulation campaigns. A new strategy for mesh decomposition, which considers all the aforementioned aspects, has been developed and applied to the GDI injector. The decomposition algorithm proceeds as follows:

- the grid is divided into several regions, in accordance to the decomposition constraints (layer A/R zones, attach/detach zones, static parts).
- each mesh region is decomposed into a number of subdomains, depending on the region size;
- all the face sets where dynamic layering is triggered (e.g. `bottomFaces`) are decomposed and subsets of faces are distributed among processors. For specified cell sets, cell decomposition is propagated perpendicularly to the face set using a cell-face walk algorithm, over the entire mesh region where layer addition/removal can be triggered;
- the remaining cells of the mesh are distributed among processors using non-constrained decomposition.

The decomposition strategy outlined above is very flexible, allowing for an almost perfect cell balancing over the processors with complex geometries and topological changes; for similar geometries, the steps for domain decomposition can be easily automated, thus favoring automatic case setup in optimization/validation simulations.

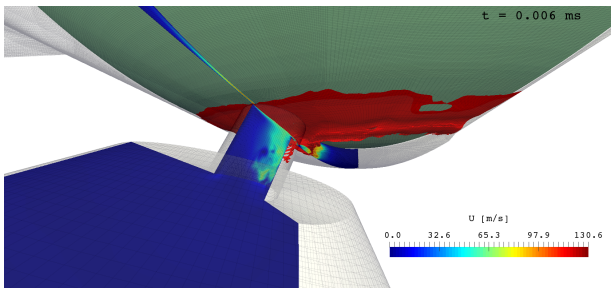

Figure 10: Snapshot of velocity field and fuel/vapor interface at $t = 6$ μs ASOI in the nozzle region of the injector.

In Fig. 10, the operation of the cavitating flow field across the injector hole after the Start of Injection (SOI), calculated by the dynamic VOF solver, is shown. The fuel/gas interface is identified by the red isosurface at $\alpha = 0.5$. As expected, the gas velocity is very high due to the high pressure difference between the fuel and the ambient. Some ripples on the fuel surface are present at the entrance of the nozzle region: they are induced by the wall-generated turbulence, that plays an important role for the onset of cavitation. The interested reader is invited to refer to a more extensive description in [**?**].

ACKNOWLEDGMENTS

Authors would like to kindly thank Prof. Jacques Borée from ISAE-ENSMA (Institut Supérieure de l'Aérotechniqueet de l'Espace, France) for having provided the detailed set of experimental data for model validation and the LCRC (Laboratory Computing Resource Center), Argonne National Lab, for making available the computing resources through the HPC cluster Blues within the `PETSc-FOAM` project.

REFERENCES